engineering proceedings

MDPI

Proceeding Paper

Synthesis and Application of Magnesium-Based Nanoparticles for Photocatalytic Degradation of Methylene Blue in Aqueous Solution: Optimization and Kinetic Modelling †

Khumbolake Faith Ngulube [1,*], Mahmoud Nasr [1,2], Manabu Fujii [3] and Amal Abdelhaleem [1]

[1] Environmental Engineering Department, Egypt-Japan University of Science and Technology (E-JUST), Alexandria 21934, Egypt; mahmoud.nasr@ejust.edu.eg (M.N.); amal.elsonbaty@ejust.edu.eg (A.A.)
[2] Sanitary Engineering Department, Faculty of Engineering, Alexandria University, Alexandria 21544, Egypt
[3] Department of Civil and Environmental Engineering Tokyo Institute of Technology, Meguro-ku, Tokyo 152-8552, Japan; fujii.m.ah@m.titech.ac.jp
* Correspondence: khumbolake.ngulube@ejust.edu.eg
† Presented at the 2nd International Electronic Conference on Processes: Process Engineering—Current State and Future Trends (ECP 2023), 17–31 May 2023; Available online: https://ecp2023.sciforum.net/.

Abstract: Heterogeneous photocatalysis has been studied with various semiconductor materials for efficient degradation of various water pollutants. However, there is a challenge of wide band gap photocatalyst materials which limits their application under visible light irradiation. Herein, a ZnO@MgO core-shell nanocomposite was synthesized using co-precipitation and applied for photocatalytic degradation of MB dye under visible light irradiation. MB degradation was optimized using response surface methodology resulting in 95.948% and ≈91% predicted and actual MB removals, respectively, at 10 mg/L MB concentration, 1000 mg/L catalyst dose, pH 10, and time 115.7 min. The degradation kinetics were studied, and it was found that the degradation followed pseudo-first-order kinetics with a rate constant of k = 0.07593 min^{-1}. A cost benefit analysis was undertaken and the operating costs were estimated based on the optimized conditions at \$7.6/m^3 with a payback period of 3.2 years.

Keywords: magnesium oxide; methylene blue dye; photocatalytic degradation; optimization; reaction kinetics; operating costs

Citation: Ngulube, K.F.; Nasr, M.; Fujii, M.; Abdelhaleem, A. Synthesis and Application of Magnesium-Based Nanoparticles for Photocatalytic Degradation of Methylene Blue in Aqueous Solution: Optimization and Kinetic Modelling. *Eng. Proc.* **2023**, *37*, x. https://doi.org/10.3390/xxxxx
Published: 17 May 2023

1. Introduction

Methylene blue (MB), commonly used in textile industry, is a heterocyclic aromatic basic cationic dye that is highly soluble in water and forms stable solutions at room temperature. Therefore, its release into the environment has harmful effects on aquatic and human life. Its exposure in high concentrations could result in respiratory issues, abdominal disorders, blindness, and mental disorders, amongst others [1]. Aquatic life are not spared because MB causes a reduction in sunlight penetration into the marine environment [2]. This slows down photosynthetic processes of aquatic plants, resulting in low dissolved oxygen levels, ultimately killing aquatic life and affecting the marine ecosystem's balance. Hence, it is of great importance that the wastewater contaminated by MB is adequately treated to prevent its exposure to the environment.

Conventional treatment techniques such as adsorption, phytoremediation, coagulation/flocculation and others have been applied for removal of MB from aqueous solution. Due to the stable nature of MB, these have shown shortcomings in terms of their viability, impact on the environment, and effectiveness [3]. Therefore, advanced treatment techniques such as advanced oxidation processes (AOPs) are being studied for efficient removal of MB.

Heterogeneous photocatalysis is one of the most efficient AOPs that can degrade organic pollutants such as MB by generating reactive oxygen species (ROS) such as •OH from a series of oxidation and reduction reactions. ROS repeatedly attack and degrade MB by converting it into simpler molecules such a CO_2 and H_2O; and this sequence of reactions can take place at standard temperature and pressure [4]. This technique does not generate large amounts of sludge, the photocatalyst material can be cheap, non-toxic, and reusable [5], and the reaction rates are relatively high [6]. Several semiconductor materials such as ZnO and MgO have been studied as photocatalysts and have displayed reasonable photocatalytic activity. However there is still need to identify photocatalyst materials that can display more superior activity.

In this study, a ZnO@MgO core-shell nanocomposite material was synthesized, characterized and applied for the photocatalytic degradation of MB under solar simulated UV-visible light irradiation. The process was optimized using response surface methodology (RSM) and the resulting optimized conditions were used to carry out an economic analysis. To the best of our knowledge, there have been no published papers that have synthesized and applied this material.

2. Materials and Methods

2.1. Materials

Magnesium chloride hexahydrate ($MgCl_2.6H_2O$) (99%) was purchased from tekkim kimya group of companies (Turkey), Zinc sulfate heptahydrate ($ZnSO_4.7H_2O$) was purchased from el nasr pharmaceutical chemicals company in Egypt, purified sodium hydroxide pellets (NaOH) (97%) was purchased from SD fine—chem limited (India), the sulfuric acid (H_2SO_4) (97%) and methanol (CH_3OH) (99.8%) were purchased from piochem in Egypt and the methylene blue powder (MB) (99%) was purchased from alpha chemical group, Egypt.

2.2. Preparation of Methylene Blue Solution

A 500 ppm stock solution of MB dye was prepared by dissolving 500 mg of MB dye powder into 1 L of distilled water. This stock solution was stored in a cool dry environment and then diluted to the desired concentrations for use in the experimental runs.

2.3. Photocatalyst Synthesis

MgO nanoparticles were synthesized using a 0.5 M precursor solution of $MgCl_2.6H_2O$ following the method used by [7]. The obtained dried powder was then calcined in a muffle furnace at 800 °C for 3 h to obtain the MgO nanoparticles.

To synthesize the ZnO@MgO core-shell nanocomposite, the as synthesized MgO nanoparticles were dispersed into a $ZnSO_4.7H_2O$ solution and stirred vigorously to keep the MgO nanoparticles in suspension. The synthesis steps proceeded as was the case for MgO; however, the obtained white powder was calcined at 350 °C for 3 h to obtain the ZnO@MgO core-shell nanocomposite. The synthesis procedures are summarized in Figure S1.

2.4. Characterization

UV-Vis Diffuse Reflectance spectrum (UV-Vis DRS, Jasco v-570 spectrometer, Japan) analysis was carried out in order to determine the optical band gap energy of the catalysts. MB dye concentration was measured using a UV spectrophotometer (Jasco V-630 spectrophotometer, Japan) set at a wavelength of 664 nm.

2.5. Photocatalytic Degradation

2.5.1. Degradation Experiments

The photocatalytic degradation experiments involved the dilution of the MB stock solution to the desired concentration and adjusting the pH by adding NaOH or H_2SO_4 until the desired pH was achieved. The catalyst was then added into the MB solution and placed in the reactor under constant stirring in the dark for 1 h to allow for adsorption-desorption equilibrium. After adsorption-desorption equilibrium was achieved, a 2 mL sample was extracted and centrifuged to separate the catalyst from the solution and the concentration, C_o was measured. The light in the reactor was switched on and photocatalytic degradation was allowed to proceed for the desired amount of time, t, after which, another 2 mL sample was extracted and the final MB concentration, C_t was measured. MB removal, R%, was calculated using the formula given by Equation (1).

$$R\% = [(C_o - C_t)/C_o] \times 100, \quad (1)$$

2.5.2. Statistical Analysis

The experimental design and optimization of parameters was done with design expert 13 software using a box-behnken design (BBD). It was used to study the effects of four selected independent variables; A (dye concentration), B (catalyst dose), C (pH) & D (time) on MB dye removal. The BBD generated a total of 29 experimental runs comprising five center points. A second order polynomial given by Equation (2) was used to study the effects of the variables on the removal of the MB and to show how each of the variables affect each other.

$$y = c_o + \sum_{i=1}^{n} c_i x_i + \sum_{i=1}^{n-1} \sum_{j=i+1}^{n} c_{ij} x_i x_j + \sum_{i=1}^{n} c_{ii} {x_i}^2 \quad (2)$$

where y is the MB removal, n is the number of independent variables, c_o is a constant, c_i, c_{ij}, c_{ii} are the first-order constant, quadratic and linear interaction coefficients respectively, x_i and x_j are independent variables and x_i^2 is a square effect.

To verify the adequacy of the generated model and each of the independent variables, analysis of variables (ANOVA) was done, and the significance of each parameter was denoted by a p-value less than 0.05. The model significance was also verified using the coefficient of determination (R^2) values. Once the model was verified, optimization of parameters was done using numerical optimization and the degradation kinetics were studied.

3. Results and Discussion

3.1. UV-Vis DRS

An indirect Tauc plot [8] was drawn as shown in Figure 1.

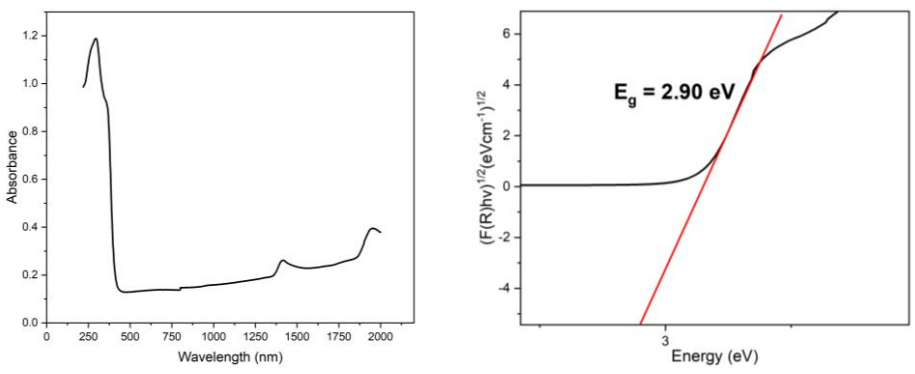

(**a**) (**b**)

Figure 1. Absorbance spectrum and Tauc plot of the ZnO@MgO core-shell nanocomposite.

The plot was derived from the UV-Vis DRS analysis results using the equation given by Equation (3);

$$[F(R)hv]^n = A(hv - E_g), \quad (3)$$

where F(R), hv, A and E_g are the Kubelka-Munk function, incident photon energy, proportionality constant and band gap energy respectively and n is ½. The extrapolation of the linear section of the graph revealed that the optical band gap energy of the ZnO@MgO core-shell nanocomposite was 2.90 eV. The theoretical band gap energy of pure ZnO has been identified in literature to be around 3.33 eV [9] whereas that of pure MgO has been identified as 4.8 eV [10]. The reduction in the energy band gap of the nanocomposite shows successful band gap narrowing by the core-shell combination of the two materials. The reduced band gap can facilitate better electron excitation within the visible light irradiation range (400–800 nm) compared with the pure ZnO and MgO separately.

3.2. Optimization, Validation and Kinetics

ANOVA was carried out (Table S1) and the model generated had a *p*-value < 0.05 and relatively high adjust and predicted R^2 values of 0.9939 and 0.9826 respectfully, which had a difference of less than 0.2. This validated the generated model as significant and suitable to be used for further analyses. The analysis also showed that all the four independent variables were significant to the degradation of the MB dye.

A second order polynomial governing the MB removal based on the independent variables was generated as shown in Equation (4).

$$R\% = 9.56 - 29.84A + 2.84B + 13.18C + 2.71D - 1.99AB - 14.05AC - 2AD + 6.05BC + 1.37BD + 8.72CD + 19.56A^2 + 1.43B^2 - 1.40C^2 + 1.01D^2, \quad (4)$$

Numerical optimization of the variables was carried out by maximizing the desired MB removal and reducing reaction time. The analysis generated 100 possible optimized conditions, of which the one selected displayed an MB removal of 95.948% in 115.7 min, for dye concentration 10 mg/L, catalyst dose of 1000 mg/L and pH 10. The generated contour plots showing the interactions of the independent variables are shown in Figure S2.

A validation run was carried out at the optimized conditions and a removal efficiency of 90.858% was achieved. 2 mL samples were extracted and analyzed at 15 min intervals and the C/C_o curve was plotted as shown in Figure 2a. The degradation kinetics were then studied in order to determine the reaction rate constant, where the MB removal was checked for fitness with zero-order, half-order, first-order and second-order degradation kinetics.

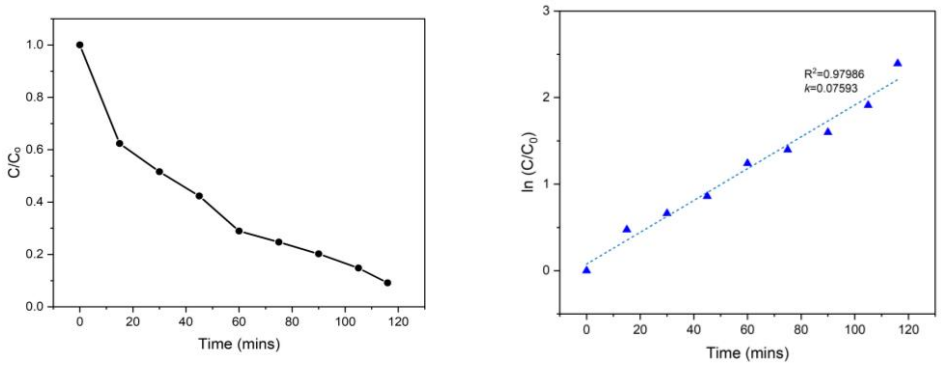

(**a**) (**b**)

Figure 3. (**a**) MB removal, (**b**) pseudo first-order degradation Kinetics [Reaction conditions: MB concentration = 10 mg/L, catalyst dose ≈ 1000 mg/L, pH = 10 and time = 115.7 min].

The reaction rate constant(s), k, were calculated as the slopes of the zero-order, half-order, first-order and second-order kinetics curves given by the equations in Table S2 [11].

The R^2 values of each model showed that the MB removal in this study was compatible with pseudo first-order degradation kinetics (Figure 2b) with a reaction rate constant of 0.07593 min^{-1}.

3.3. Effects of Operational Parameters

The effect of the independent variables on the removal of the MB dye was studied and the graphs generated are shown in Figure S3.

3.3.1. Effect of Dye Concentration

The effect change in MB concentration was investigated by varying the dye concentration from 10 to 100 mg/L (Figure S3a). As the MB concentration was increased, the removal efficiency decreased. The decrease in the removal efficiency could be as a result of the blocking of active sites on the photocatalyst surface with increased dye concentrations [12] which results in reduced interactions between photons and active sites; and ultimately limits the generation of ROS for MB degradation. Another reason for this reduction is that when the dye concentration is high, light penetration to the photocatalyst surface is reduced [13]. Photon energy will be absorbed by the dye molecules, instead of the catalyst material. Additionally, the newly generated intermediates that will be formed during the photocatalytic reaction will compete with the parent dye molecules for the reactive radicals.

3.3.2. Effect of Catalyst Dose

In order to study the effect of catalyst dosage on the photocatalytic degradation of MB dye, the concentration of ZnO@MgO in the degradation experiments was varied from 100 to 1000 mg/L (Figure S3b). It was observed that the removal efficiency increased as catalyst dosage was increased from 100 mg/L to 1000mg/L. The increment in removal efficiency can be attributed to the increased number of active sites at higher catalyst dosages. This increase allows for more catalyst-photon interactions, followed by the generation of more ROS to degrade the MB dye [12].

3.3.3. Effect of pH

The effect of pH on the photocatalytic removal of the dye was studied at pH ranges of 3 to 10 (Figure S3c). The results showed that the removal efficiencies improved with an increase in the solution pH value. The trend displayed is acceptable given that MB dye is a cationic dye (positively charged) and when the solution pH exceeds the point of zero charge (PZC) pH of 10.44 (Figure S4), the catalyst surface charge becomes negative [14]. When the catalyst was added to a neutral MB dye solution, the pH increased to about 11, and when the initial MB concentration is set to 10, the solution pH would further increase to about 11.55, making the surface charge of the catalyst negative. The opposite charge of the catalyst to the MB dye molecules will result in more attraction of the MB to the catalyst surface. This attraction will increase MB-ROS interactions, resulting in higher removal efficiencies.

3.3.4. Effect of Time

The effect of time on the MB removal was studied by varying time between 60 and 180 min (Figure S3d). It was observed that the MB removal and time displayed a directly proportional relationship. Further increase in the reaction time caused an obvious increase in the MB removal efficiency. This is due to prolonged contact time [15] between the generated ROS on the photocatalyst surface and the MB dye.

3.4. Economic Evaluation

In order to estimate the feasibility of the up-scale synthesis and application of the ZnO@MgO core-shell nanocomposite for dyes removal, an economic analysis was carried out where the capital costs, operating costs and possible revenues were estimated as shown in Table S3 based on the optimized parameters of the lab experiments. The analysis assumes a daily wastewater inflow of 80m^3 which is suitable for a roughly medium size treatment plant.

The capital costs included the costs of the photocatalytic reactor and all its components, catalyst synthesis apparatus, plant infrastructure construction costs, contractor charges and contingencies calculated using the equation given in Table S4. The total capital costs were then estimated to about $2,941,149.22.

The operational costs were also estimated and comprised expenses such as electricity, cost of chemicals, water bills, statutory obligations such as taxes, workers' salaries as well as equipment repair and maintenance costs. The total annual operational costs estimate amounted to $182,443.56 which gave a running cost of $7.6/m^3 of influent water. The possible revenues identified were the removal of the dye from the water, the sale of the synthesized catalyst material as well as the reuse of the treated effluent for on-site applications. The estimate of the total revenues was $1,097,416.73. Finally, the capital costs, operational costs and the revenues were used to derive the payback period and it was estimated at 3.2 years.

Supplementary Materials: The following supporting information can be downloaded at: www.mdpi.com/xxx/s1, Figure S1: Catalyst synthesis procedure; Figure S2: Interaction of parameters towards MB removal; Figure S3: Effect of operational parameters on MB removal (a) effect of dye concentration; (b) effect of catalyst dose; (c) effect of pH; (d) effect of time; Figure S4: PZC of the core-shell nanocomposite; Table S1: ANOVA Table; Table S2: Equations governing the kinetic modelling; Table S3: Cost benefit analysis; Table S4: Capital cost estimation formulae.

Author Contributions: Conceptualization, K.F.N., M.N. and A.A.; methodology, K.F.N.; software, M.N.; validation, K.F.N.; formal analysis, K.F.N.; investigation, K.F.N.; resources, M.N., A.A., and M.F.; data curation, K.F.N.; writing—original draft preparation, K.F.N.; writing—review and editing, K.F.N., M.N. and A.A.; visualization, K.F.N.; supervision, M.N., A.A. and M.F.; project administration, M.N. and A.A. All authors have read and agreed to the published version of the manuscript.

Funding: This research received no external funding.

Data Availability Statement: The data presented in this study are available upon request from the corresponding author.

Acknowledgments: The authors wish to acknowledge TICAD 7 for the scholarship of the researcher as well as JICA and E-JUST for all equipment used throughout the research.

Conflicts of Interest: The authors declare no conflict of interest.

References

1. Cusioli, L.F.; Quesada, H.B.; Baptista, A.T.A.; Gomes, R.G.; Bergamasco, R. Soybean hulls as a low-cost biosorbent for removal of methylene blue contaminant. *Environ. Prog. Sustain. Energy* **2020**, *39*, e13328. https://doi.org/10.1002/ep.13328.
2. Ebi Ebi, O.; Falilat Taiwo, A.; Tunde Folorunsho, A. Kinetic Modelling of the Biosorption of Methylene Blue onto Wild Melon (Lagenariasphaerica). *Am. J. Chem. Eng.* **2018**, *6*, 126–134. https://doi.org/10.11648/j.ajche.20180606.12.
3. Crini, G.; Lichtfouse, E. Advantages and disadvantages of techniques used for wastewater treatment. *Environ. Chem. Lett.* **2019**, *17*, 145–155. https://doi.org/10.1007/s10311-018-0785-9.
4. Ahmed, S.N.; Haider, W. Heterogeneous photocatalysis and its potential applications in water and wastewater treatment: A review. *Nanotechnology* **2018**, *29*, 342001. https://doi.org/10.1088/1361-6528/aac6ea.
5. Karim, M.A.H.; Aziz, K.H.H.; Omer, K.M.; Salih, Y.M.; Mustafa, F.; Rahman, K.O.; Mohammad, Y. Degradation of aqueous organic dye pollutants by heterogeneous photo-assisted Fenton-like process using natural mineral activator: Parameter optimization and degradation kinetics. *IOP Conf. Ser. Earth Environ. Sci.* **2021**, *958*, 012011. https://doi.org/10.1088/1755-1315/958/1/012011.
6. Advanced Oxidation Processes (AOP) | Spartan. *Spartan Water Treat.*

7. Rao, K.G.; Ashok, C.H.; Rao, K.V.; Chakra, C.H.S. Structural properties of MgO Nanoparticles : Synthesized by Co-Precipitation Technique Structural properties of MgO Nanoparticles: Synthesized by Co-Precipitation Technique. *Int. J. Sci. Res.* **2014**, *3*, 43–46.
8. Makuła, P.; Pacia, M.; Macyk, W. How To Correctly Determine the Band Gap Energy of Modified Semiconductor Photocatalysts Based on UV–Vis Spectra. *J. Phys. Chem. Lett.* **2018**, *9*, 6814–6817. https://doi.org/10.1021/acs.jpclett.8b02892.
9. Kamarulzaman, N.; Kasim, M.F.; Rusdi, R. Band Gap Narrowing and Widening of ZnO Nanostructures and Doped Materials. *Nanoscale Res. Lett.* **2015**, *10*, 346. https://doi.org/10.1186/s11671-015-1034-9.
10. Almontasser, A.; Parveen, A.; Azam, A. Synthesis, Characterization and antibacterial activity of Magnesium Oxide (MgO) nanoparticles. *IOP Conf. Ser. Mater. Sci. Eng.* **2019**, *577*, 012051. https://doi.org/10.1088/1757-899X/577/1/012051.
11. Mensah, K.; Samy, M.; Ezz, H.; Elkady, M.; Shokry, H. Utilization of iron waste from steel industries in persulfate activation for effective degradation of dye solutions. *J. Environ. Manag.* **2022**, *314*, 115108. https://doi.org/10.1016/j.jenvman.2022.115108.
12. Sadeghi, M.; Heydari, M.; Javanbakht, V. Photocatalytic and photo-fenton processes by magnetic nanophotocatalysts for efficient dye removal. *J. Mater. Sci. Mater. Electron.* **2021**, *32*, 5065–5081. https://doi.org/10.1007/s10854-021-05241-w.
13. Akpan, U.G.; Hameed, B.H. Parameters affecting the photocatalytic degradation of dyes using TiO2-based photocatalysts: A review. *J. Hazard. Mater.* **2009**, *170*, 520–529. https://doi.org/10.1016/j.jhazmat.2009.05.039.
14. Alkaim, A.; Aljeboree, A.; ALRAZAQ, N.A.; Jaafer, S.; Hussein, F.; LILO, A.J. Effect of pH on Adsorption and Photocatalytic Degradation Efficiency of Different Catalysts on Removal of Methylene Blue. *Asian J. Chem.* **2014**, *26*, 8445–8448. https://doi.org/10.14233/ajchem.2014.17908.
15. Kumar, A.; Pandey, G. The photocatalytic degradation of Methyl Green in presence of Visible light with photoactive Ni 0.10 :La 0.05 :TiO 2 nanocomposites. *IOSR J. Appl. Chem.* **2017**, *10*, 31–44. https://doi.org/10.9790/5736-1009013144.

Supplementary Materials

For

Synthesis and Application of Magnesium-Based Nanoparticles for Photocatalytic Degradation of Methylene Blue in Aqueous Solution: Optimization and Kinetic Modelling †

Khumbolake Faith Ngulube [1,*], Mahmoud Nasr [1,2], Manabu Fujii [3] and Amal Abdelhaleem [1]

[1] Environmental Engineering Department, Egypt-Japan University of Science and Technology (E-JUST), Alexandria 21934, Egypt; mahmoud.nasr@ejust.edu.eg (M.N.); amal.elsonbaty@ejust.edu.eg (A.A.)
[2] Sanitary Engineering Department, Faculty of Engineering, Alexandria University, Alexandria 21544, Egypt
[3] Department of Civil and Environmental Engineering Tokyo Institute of Technology, Meguro-ku, Tokyo 152-8552, Japan; fujii.m.ah@m.titech.ac.jp
* Correspondence: khumbolake.ngulube@ejust.edu.eg

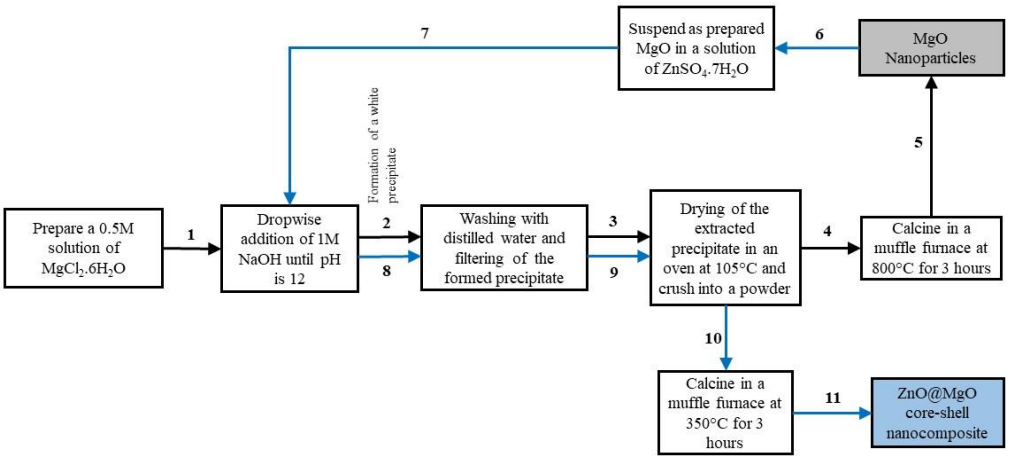

Figure S1. Catalyst Synthesis Procedure.

Table S1. ANOVA Table.

Source	Sum of Squares	df	Mean Square	F-Value	*p*-Value	
Model	16,927.30	14	1209.09	324.54	<0.0001	significant
A-Dye Conc.	10,687.08	1	10,687.08	2868.62	<0.0001	
B-Catalyst Dose	96.65	1	96.65	25.94	0.0002	
C-pH	2084.83	1	2084.83	559.61	<0.0001	
D-Time	88.13	1	88.13	23.65	0.0003	
AB	15.77	1	15.77	4.23	0.0587	
AC	789.96	1	789.96	212.04	<0.0001	
AD	15.99	1	15.99	4.29	0.0572	
BC	146.57	1	146.57	39.34	<0.0001	
BD	7.49	1	7.49	2.01	0.1780	
CD	304.33	1	304.33	81.69	<0.0001	
A^2	2480.93	1	2480.93	665.93	<0.0001	
B^2	13.31	1	13.31	3.57	0.0796	
C^2	12.77	1	12.77	3.43	0.0853	
D^2	6.66	1	6.66	1.79	0.2025	

R^2	0.9969
Adjusted R^2	0.9939
Predicted R^2	0.9826

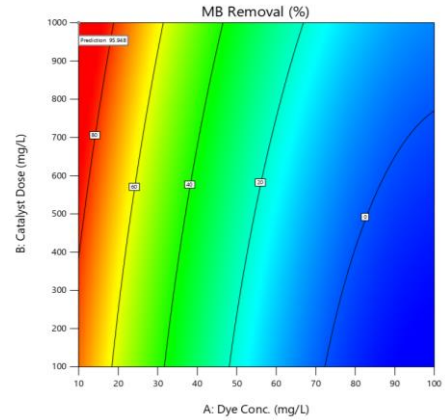

(**a**)

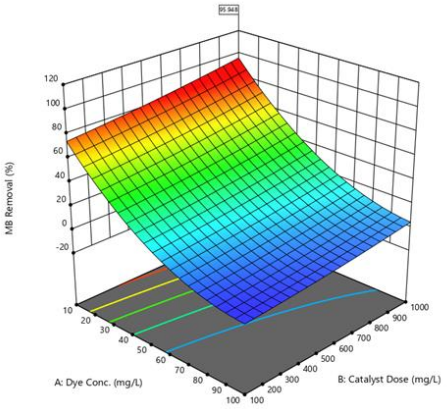

(**b**)

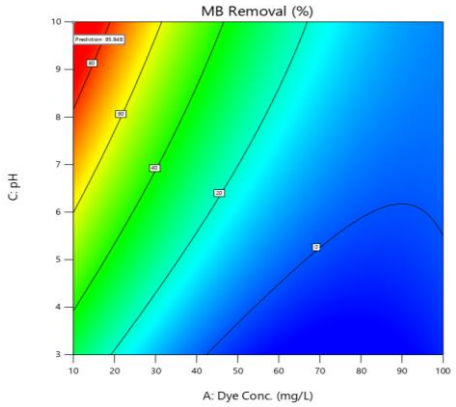

(**c**)

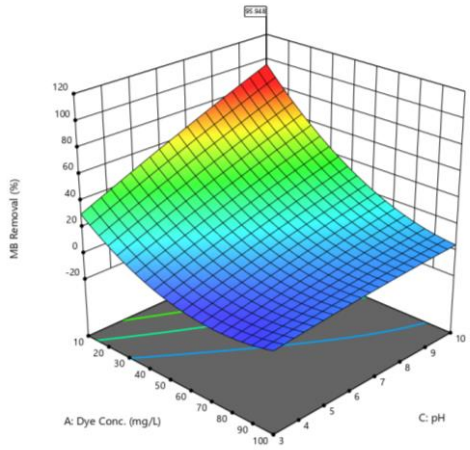

(**d**)

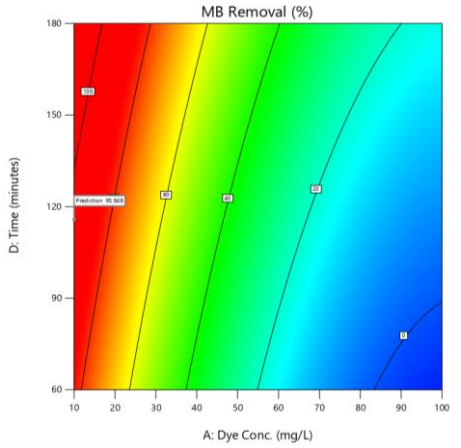

(**e**)

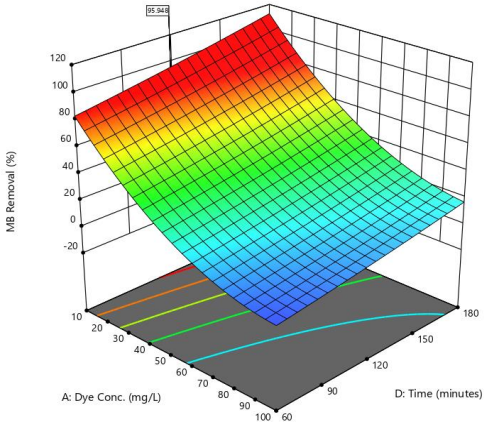

(**f**)

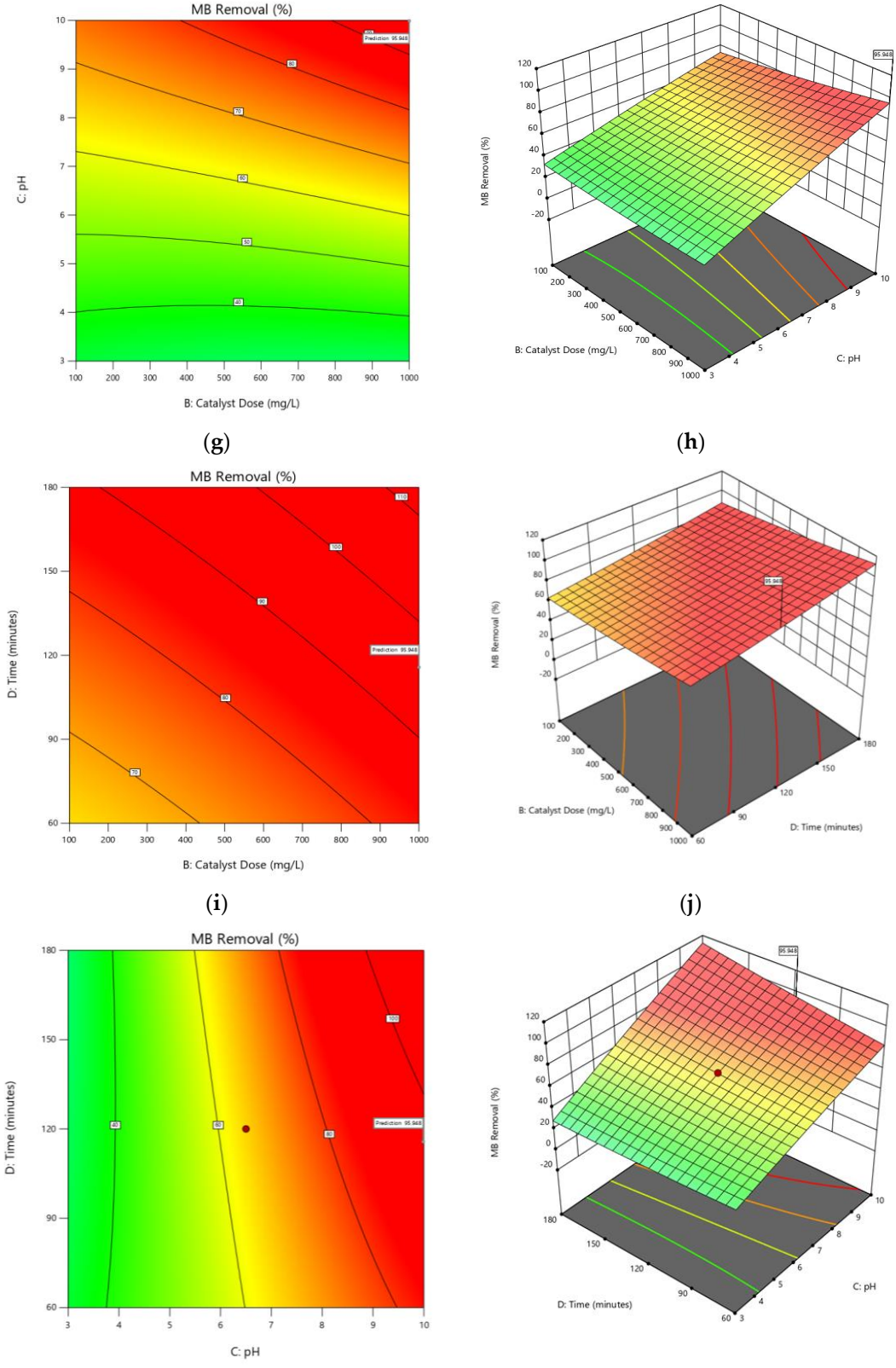

Figure S2. Interaction of parameters towards MB removal.

Table S2. Equations governing the kinetic modelling.

Kinetic Model	Governing Equation
Zero-order	$-k_0t = C_t - C_0$,
Half-order	$-k_{0.5}t = 2(C_t^{0.5} - C_0^{0.5})$,
First-order	$-k_1t = \ln(C_t/C_0)$,
Second-order	$-k_2t = (1/C_t) - (1/C_0)$,

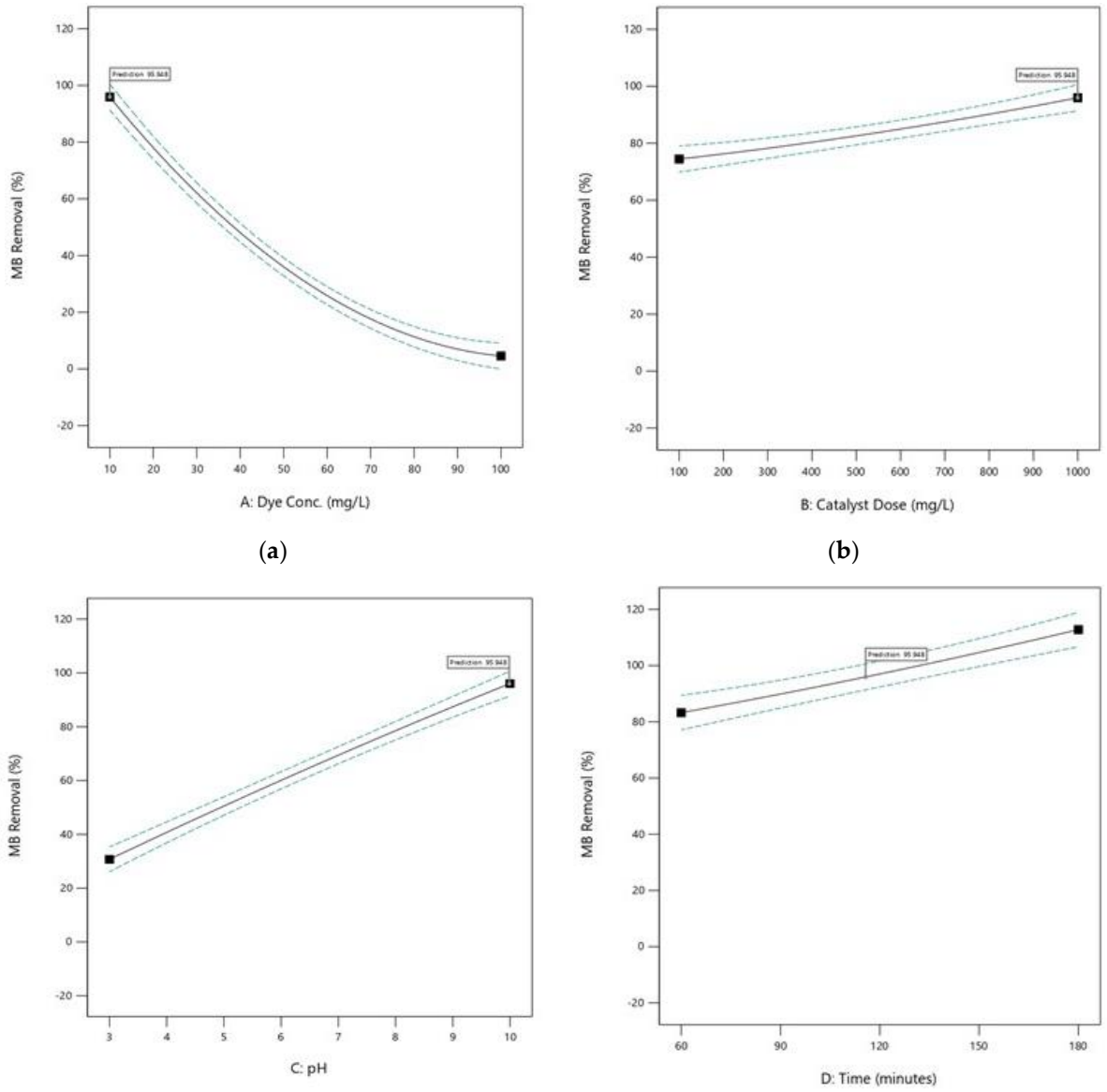

(**a**) (**b**)

(**c**) (**d**)

Figure S3. Effect of operational parameters on MB removal (**a**) effect of dye concentration; (**b**) effect of catalyst dose; (**c**) effect of pH; (**d**) effect of time.

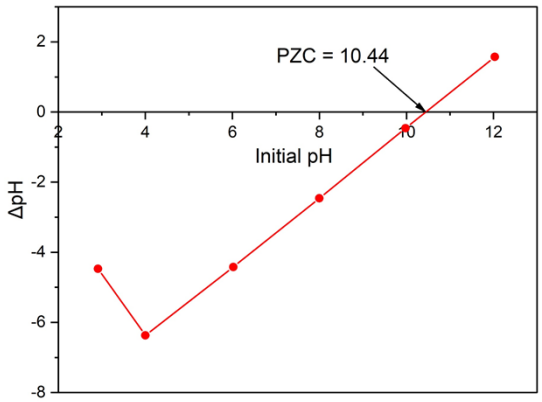

Figure S4. PZC of the core-shell nanocomposite.

Table S3. Cost benefit analysis.

	Description	%	Unit	Cost
Capital Costs	Land acquisition	1.48	$	43,465.26
	Photocatalysis reactor tank	11.69	$	345,444.85
	Treated effluent and used up catalyst removal pumps	5.01	$	148,047.79
	Treated water tanks	3.34	$	98,698.53
	Used up photocatalyst tanks	1.67	$	49,349.26
	Pipes and valves	1.00	$	29,609.56
	UV Lamps	6.68	$	197,397.06
	Stirrer Motor	4.01	$	118,438.23
	Catalyst synthesis chambers	23.37	$	608,813.01
	Filtration and washing tank	0.51	$	7,377.05
	Calcination furnace	0.45	$	6,533.33
	Construction works including installations of tanks, piping, valves and electrical works and site works	13.36	$	394,794.11
	Contractor charges	7.01	$	207,266.91
	Engineering consultancy charges	8.06	$	238,356.94
	Contingencies and other	12.37	$	365,480.65
	TOTAL CAPITAL COSTS	100.00	**$**	**2,941,149.22**
Operating Costs	Catalyst synthesis chemicals	17.21	$/year	31,394.18
	Treatment chemicals	6.63	$/year	12,096.00
	Electricity consumption by UV lamps, pumps, stirrer motor ($0.195/m^3)	2.57	$/year	4,680.00
	Catalyst synthesis and regeneration water	1.05	$/year	1,921.67
	Repair and maintenance of all equipment	24.18	$/year	44,117.24
	Government taxes	16.12	$/year	29,411.49
	Workers remuneration	32.24	$/year	58,822.98
	TOTAL OPERATING COSTS	**100**	**$/year**	**182,443.56**
Revenues	Treated water reuse on-site		$/year	5,015.36
	Dye colour removal		$/year	896,441.37
	Sale of synthesized catalyst materials		$/year	195,960.00

Table S4. Capital cost estimation formulae.

Item	Formula
Infrastructure construction works including Piping, valves and electrical works and site works	CC
Photocatalytic reactor and mechanical equipment	CC/0.4
Sub-total	CC + CC/0.4 = R
Contractor charges	0.15R
Sub-total	1.15R = S
Engineering consultancy charges	0.15S
Sub-total	1.15S = T
Contingency Allowance	0.2T